Development of Yttrium-Doped BaF$_2$ Crystals for Future HEP Experiments

Chen Hu, *Member, IEEE,* Chao Xu, Liyuan Zhang, *Member, IEEE,* Qinghui Zhang, and Ren-Yuan Zhu , *Senior Member, IEEE*

Abstract—Because of their ultrafast scintillation with subnanosecond decay time, barium fluoride (BaF$_2$) crystals have attracted broad interest in the high energy physics and nuclear physics communities. One crucial issue, however, is its slow scintillation component with 600-ns decay time, which causes pile-up in a high rate environment. Previous studies show that the slow component can be suppressed effectively by rare earth doping. In this paper, we report investigations on a set of Φ 18 × 21 mm^3 BaF$_2$ cylinders doped with different yttrium levels grown at Beijing Glass Research Institute (BGRI), from which the optimized yttrium doping level was determined. A Φ 40 × 160 mm^3 BaF$_2$ ingot with 5 atomic % (at.%) yttrium doping was consequently grown at BGRI and was used to cut one 25 × 25 × 100 mm^3 crystal and several thin slices. Their optical and scintillation properties were measured at Caltech. The results show that yttrium doping effectively suppresses the slow component while maintaining its ultrafast light unchanged. Research and development will continue to develop large-size BaF$_2$:Y crystals with improved optical quality for a fast BaF$_2$:Y crystal calorimeter for Mu2e-II.

Index Terms—Barium fluoride (BaF$_2$), slow scintillation component suppression, yttrium doping.

I. INTRODUCTION

BECAUSE of its ultrafast scintillation component peaked at 220 nm with subnanosecond decay time, barium fluoride (BaF$_2$) crystals have attracted broad interest in the high energy physics (HEP) and nuclear physics community. Early investigations [1]–[3] revealed that the ultrafast intrinsic luminescence in BaF$_2$ can be ascribed to the crossluminescence (CL), which is due to a radiative recombination of electrons from the F$^-$ 2p-valence band with holes in the Ba^{2+} 5p-core band. One crucial issue, however, is its slow scintillation component peaked at 300 nm with a 600-ns decay time and five times intensity of the ultrafast component, which causes pile-up for high rate applications.

A BaF$_2$ crystal calorimeter was baselined for the Mu2e-I experiment [4] and was replaced by an undoped CsI crystal calorimeter exactly due to this issue [5]. It is known that undoped CsI survives the Mu2e-I radiation environment with an ionization dose up to a few tens krad but not beyond 100 krad expected by Mu2e-II. On the other hand, BaF$_2$ is found to have much better radiation hardness against ionization dose [6], protons [7], and neutrons [8]. Research and development was thus carried out along two directions to suppress the slow signal in BaF$_2$ readout: 1) selective doping in BaF$_2$ to suppress the slow component [9]–[13], [15]–[19] and 2) development of an ultrafast solar-blind photodetector, which is sensitive to the fast component but not the slow component [20], [21]. This paper summarizes our investigations on the yttrium-doped BaF$_2$ (BaF$_2$:Y) crystals grown at the Beijing Glass Research Institute (BGRI), while investigation on BaF$_2$:Y crystals grown at the Shanghai Institute of Ceramics (SIC) is published elsewhere [15], [22].

Early studies attributed the slow scintillation component to long-lived triplet states of self-trapped excitons (STEs) [23] and pointed out that an effective suppression of the STE luminescence in BaF$_2$ may be achieved at room temperature by applying rare earth ions doping [16], [18], [24]–[26] through energy transfer from STE to quench emission centers. Our previous studies [13]–[15], [22], [27] also show that the slow component may be suppressed by La, La/Ce, and yttrium doping. Compared to other rare earth dopants, two advantages for yttrium doping are: 1) effective suppression of the slow component and 2) no Y^{3+}-related emission due to fully occupied p and d orbits, so no additional slow component is present. The first 190-mm long BaF$_2$:Y crystal with 1% yttrium doping was grown at SIC [15]. It, however, has poor optical quality, fast/slow (F/S) ratio, and light response uniformity (LRU). Optimization of optical quality and yttrium doping level is thus crucial for this development.

In this paper, we present investigations on a set of Φ18 × 21 mm^3 BaF$_2$ cylinders doped with different yttrium levels grown at BGRI, from which the optimized yttrium doping level was determined. A Φ40 × 160 mm^3 BaF$_2$:Y ingot was consequently grown with the optimized yttrium doping level at BGRI and was used to cut one large BaF$_2$:Y crystal of 25 × 25 × 100 mm^3 and several thin slices. Their optical and scintillation properties, such as transmittance, light output (LO), F/S, and LRU, were measured at the Caltech HEP Crystal Laboratory. The potential application of, and our future development plan for, BaF$_2$:Y crystals is also discussed.

II. SAMPLES AND EXPERIMENTAL DETAILS

Fig. 1 shows the nine BaF$_2$ cylinders of Φ18 × 21 mm^3 investigated. They were grown at BGRI with Y^{3+} doping
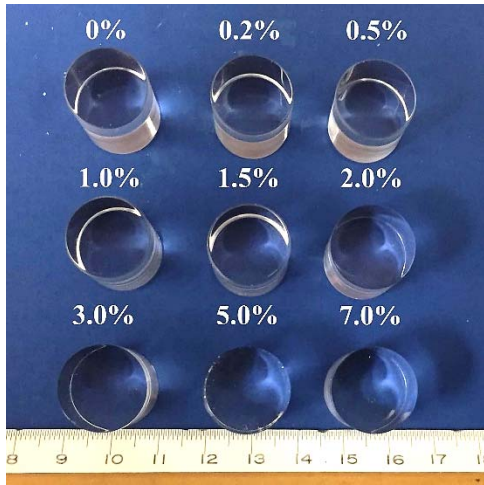
Fig. 1.   Photographs of nine BaF₂ crystal cylinders of $\Phi 18 \times 21$ mm³ grown at BGRI with 0 at.%, 0.2 at.%, 0.5 at.%, 1.0 at.%, 1.5 at.%, 2.0 at.%, 3.0 at.%, 5.0 at.%, and 7.0 at.% Y-doping.
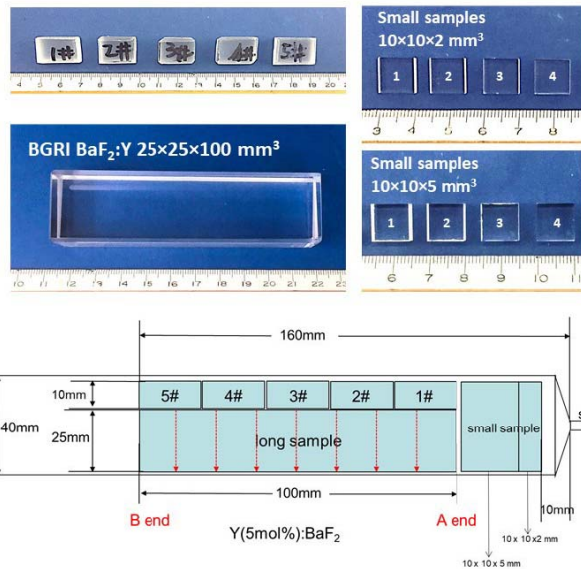

Fig. 2.   Photographs of one BaF₂:Y crystal of $25 \times 25 \times 100$ mm³ and eight small samples of $10 \times 10 \times 2$ and $10 \times 10 \times 5$ mm³ as well as five small samples with a rough surface finish (top). A schematic showing their locations in an ingot of $\Phi 40 \times 160$ mm³ grown at BGRI with 5 at.% Y-doping (bottom).

levels of 0 atomic % (at.%), 0.2 at.%, 0.5 at.%, 1.0 at.%, 1.5 at.%, 2.0 at.%, 3.0 at.%, 5.0 at.%, and 7.0 at.%. Fig. 2 shows the photographs of one BaF₂:Y crystal of $25 \times 25 \times 100$ mm³ and four small samples each of $10 \times 10 \times 2$ mm³ and $10 \times 10 \times 5$ mm³ with all surfaces polished. These samples were cut from an ingot of $\Phi 40 \times 160$ mm³ grown at BGRI with 5 at.% Y-doping. The figure also shows the locations of these samples in the ingot. Five additional small samples of $10 \times 12 \times 18$ mm³ without surface polishing were also cut adjacent to the 100-mm long crystal. They are designated as 1#–5# in Fig. 2.

X-ray-excited luminescence (XEL) spectra were measured with samples placed in a sample compartment of an Edinburgh Instruments FLSP 920 spectrophotometer with a slit width
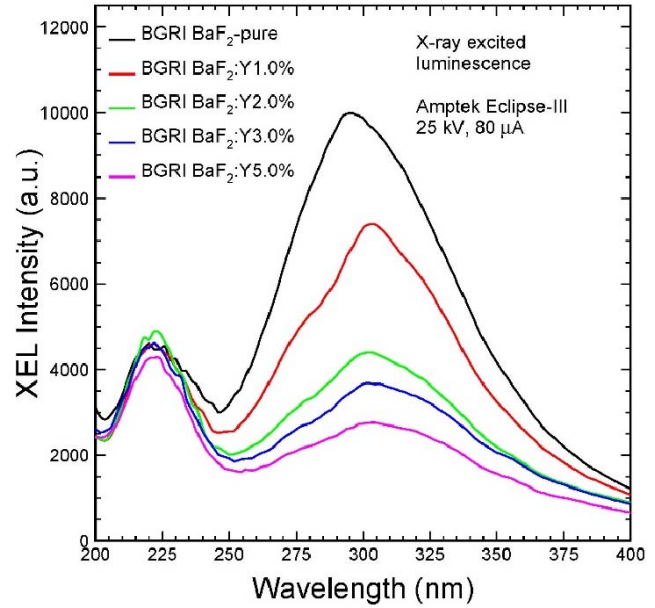

Fig. 3.   XEL spectra for five BaF₂ cylinders with various yttrium doping levels.

of 10 nm. X-rays generated by an Amptek Eclipse-III X-ray tube with a high voltage of 25 kV and a current of 80 μA were used to excite the samples. Transmittance spectra were measured with a PerkinElmer Lambda 950 spectrophotometer with 0.15% precision. The LO was measured by a Hamamatsu R2059 photomultiplier tube (PMT) with a grease coupling to the sample excited by 0.511-MeV γ-rays from a ^{22}Na source with a coincidence trigger. The systematic uncertainty of the LO measurement is about 1%.

III. RESULTS AND DISCUSSION

A. Performance of the Cylinder Samples

Figs. 3–5 shows the comparison of XEL and transmittance spectra as well as LO as a function of integration time, respectively, for five BaF₂ crystal cylinders of $\Phi 18 \times 21$ mm³, including an undoped BaF₂ and four BaF₂:Y samples with yttrium doping levels of 1 at.%, 2 at.%, 3 at.%, and 5 at.%.

Fig. 3 shows the two broad XEL peaks observed in all samples. While the intensities of the fast emission peak around 220 nm with subnanosecond decay time are consistent, the intensities of the slow emission peaked at 300 nm with 300-ns decay time are reduced when the yttrium doping level increases. This indicates that yttrium doping suppresses only the slow component.

Fig. 4 shows the transmittance spectra (solid lines) measured along a 21-mm light path for all samples. The figure also shows the XEL spectrum measured for the BaF₂:Y5% sample (dashed lines) and the numerical values of the emission weighted longitudinal transmittance (EWLT) at 220 and 300 nm, which were integrated from 200 to 250 nm and 250 to 400 nm, respectively. Two absorption bands peaked at 204 and 290 nm are clearly observed in all samples, which was attributed to the La³⁺ and Ce³⁺ contamination, respectively [13]. Since the 290-nm absorption was also
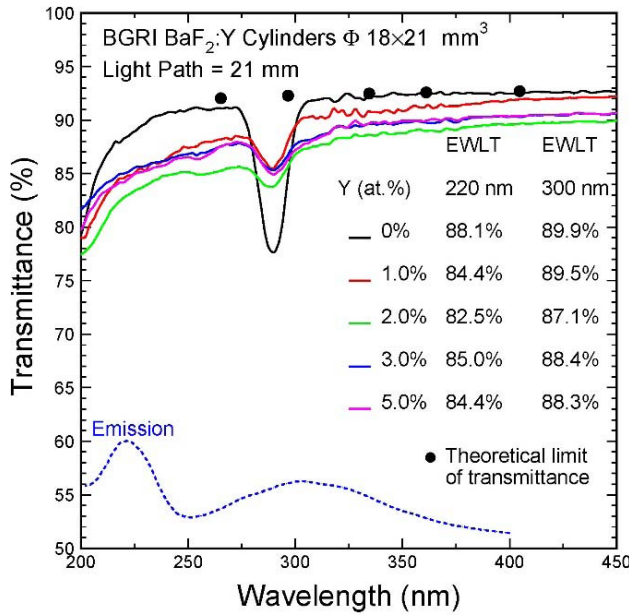
Fig. 4. Transmittance spectra for five BaF_2 cylinders with various yttrium doping levels together with emission spectra.
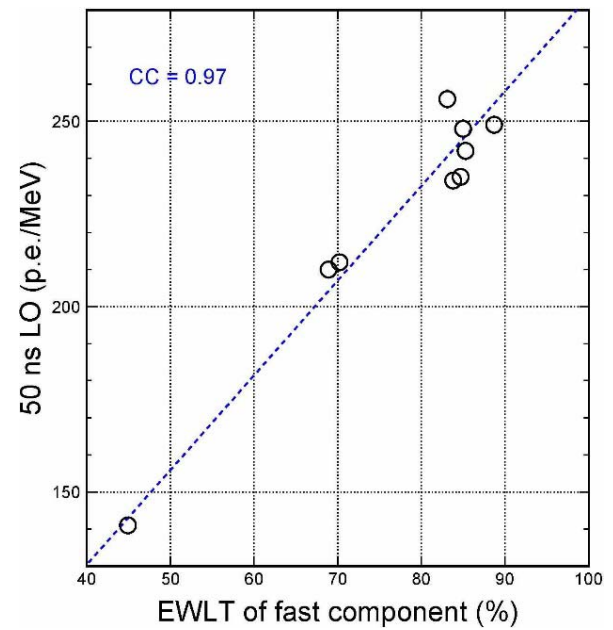

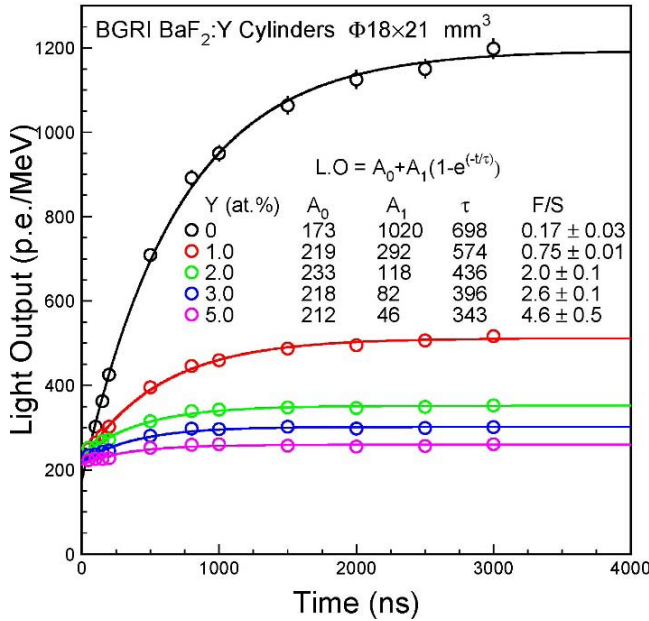Fig. 6. Correlation between EWLT of the fast component and LO in 50 ns.

Fig. 5. LO as a function of the integration time for five BaF_2 cylinders with various yttrium doping levels.
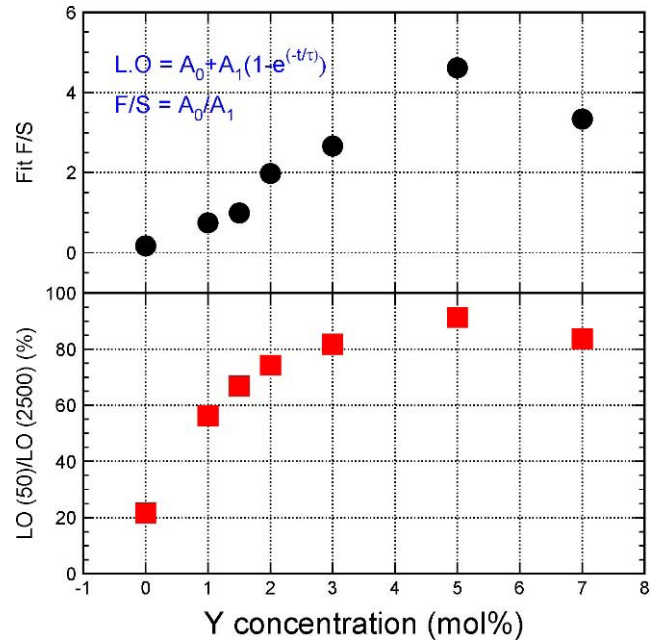

Fig. 7. LO as a function of the yttrium concentration for eight BaF_2 cylinders with various Y^{3+} doping levels.

observed in BaF_2:La samples with a cerium contamination level of less than 7 ppm, it was also attributed to other impurities and structure-related defects, such as oxygen contamination introduced during the growth process [13]. Early studies [24] also suggested that absorptions at 290 nm were significant in BaF_2 crystals with a Ce^{3+} contamination at a level as low as 10 ppm.

Fig. 5 shows the LO as a function of integration time for these samples with corresponding exponential fit to an ultrafast component (A_0) and a slow component (A_1). While more than 200 p.e./MeV is found for the ultrafast component in all doped

samples, the amplitude of the slow component is found to be reduced dramatically from 1020 p.e./MeV for the undoped sample to 46 p.e./MeV for the sample with 5.0 at.% yttrium doping, showing an effective slow component suppression.

Fig. 6 shows a correlation between the LO in the 50-ns gate and the EWLT values at 220 nm with an excellent correlation coefficient of 97%. This observation indicates that the fast LO is correlated with the crystal's optical quality at 220 nm.

The top and bottom plots in Fig. 7 show, respectively, the ratios of fast/slow and fast/total as a function of the yttrium doping concentration for seven samples. These ratios
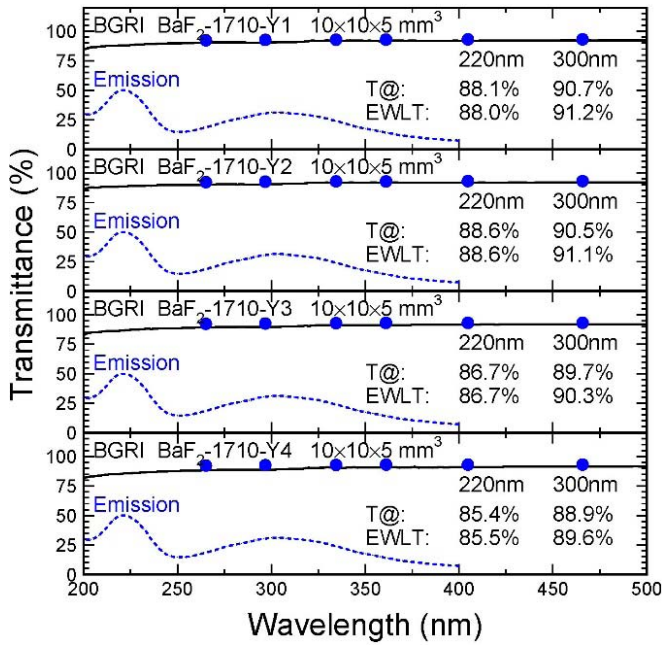
Fig. 8. Transmittance for four plate samples of $10 \times 10 \times 5$ mm^3.

Fig. 9. LO and decay kinetics for four plate samples of $10 \times 10 \times 5$ mm^3.

are defined, respectively, as A_0/A_1 in Fig. 5 and the ratio between the LO values measured in 50 and 2500 ns. The best F/S and F/T ratios of 4.6% and 91% are achieved with 5.0 at.% yttrium doping, respectively.

B. Performance of the Thin Slice Samples

Following the above-mentioned observations, a BaF$_2$:Y ingot of $\Phi 40 \times 160$ mm^3 was grown at BGRI with 5 at.% yttrium doping. Fig. 8 shows the transmittance spectra for four small BaF$_2$:Y plates of $10 \times 10 \times 5$ mm^3 cut close to the seed end. The figure also shows the emission spectrum and the numerical values of the EWLT at 220 and 300 nm. All samples show very good transmittance at both visible and ultraviolet wavelength ranges, indicating an excellent optical quality.

Fig. 9 shows the LO as a function of integration time for these four samples. The observed F/S ratio, defined as A_0/A_1, is more than 3:1 in most samples. Compared to the typical F/S ratio of 1:5 for undoped BaF$_2$, the slow component in BaF$_2$:Y crystals is significantly suppressed.

Fig. 10 shows an excellent correlation between the LO values in 50 ns and the ELWT values at 220 nm for four samples each of $10 \times 10 \times 5$ mm^3 and $10 \times 10 \times 2$ mm^3 from the same ingot (see Fig. 2 for the locations). The data show a high correlation coefficient of 95%, confirming that good optical quality in the ultraviolet range is crucial for the ultrafast light in BaF$_2$:Y.

C. Performance of the 100-mm Long Crystal

Figs. 11 and 12 show the longitudinal and transverse transmittance spectra along the 100- and 25-mm light paths, respectively, for the long BaF$_2$:Y sample of $25 \times 25 \times 100$ mm^3. These figures also show the emission spectrum (dashed lines) and the numerical values of EWLT at 220 and
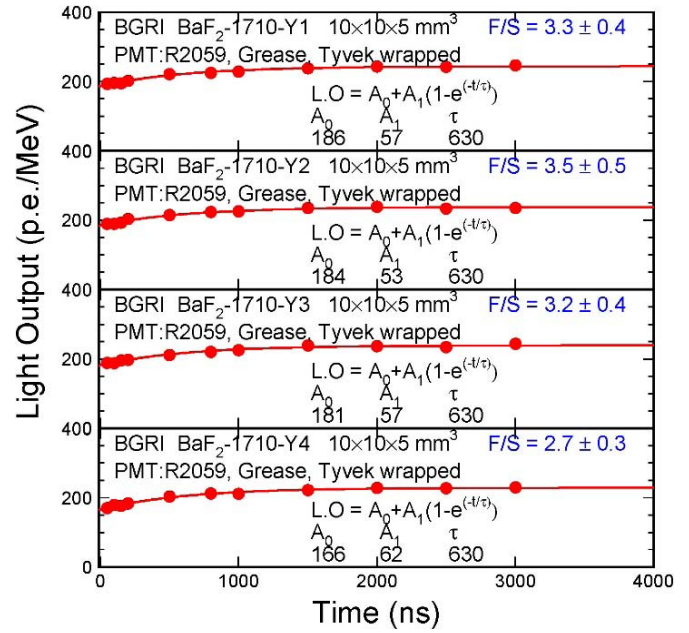

Fig. 10. Correlation between EWLT for the fast component and 50-ns LO.

300 nm. Three absorption bands peaked at 235, 255, and 290 are observed. The absorption band peaked at 290 nm was assigned to single-ion Ce^{3+} $4f$-$5d(e_g)$ transition [28], [29] and was observed in both BaF$_2$:La [13] and BaF$_2$:La/Ce [14] crystal, so that it can be attributed to either Ce^{3+} contamination or other impurities and structure-related defects, such as oxygen contamination introduced during the growth process [13]. The bands peaked at 235 and 255 nm were observed in the BaF$_2$:La/Ce crystal [14] but not in the BaF$_2$:La

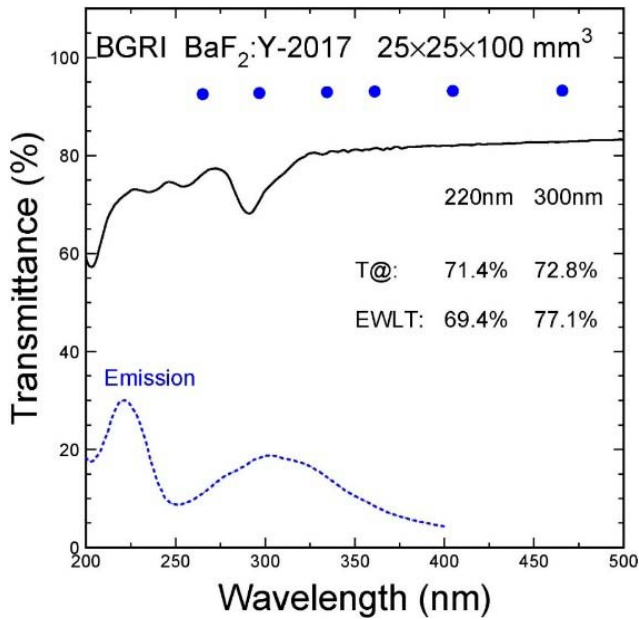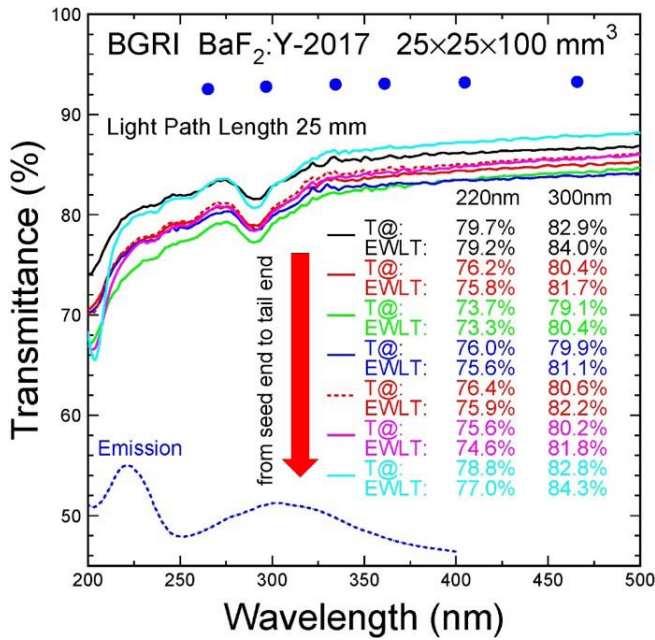Fig. 11.   Longitudinal transmittance spectrum along the 100-mm light path is shown for the BaF$_2$:Y sample of $25 \times 25 \times 100$ mm^3.
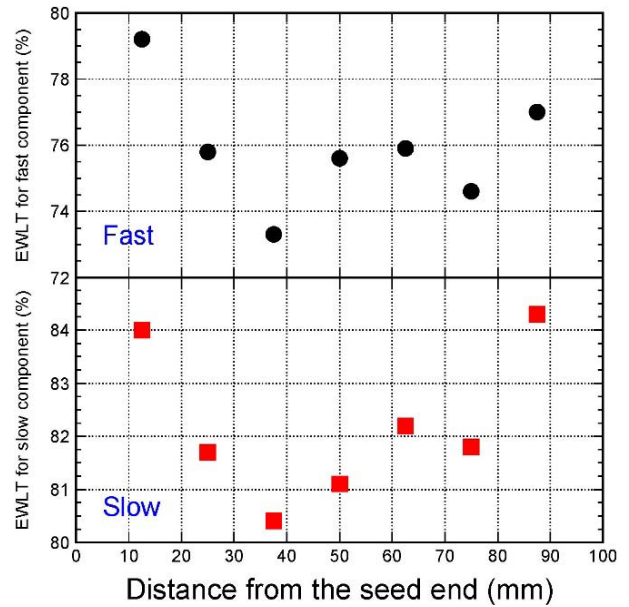

Fig. 13.   EWLT values of fast component (top) and slow component (bottom) as a function of the distance from the seed end of the BaF$_2$:Y of $25 \times 25 \times 100$ mm^3.

Fig. 12.   Transverse transmittance spectra along the 25-mm light path are shown for the BaF$_2$:Y sample of $25 \times 25 \times 100$ mm^3.
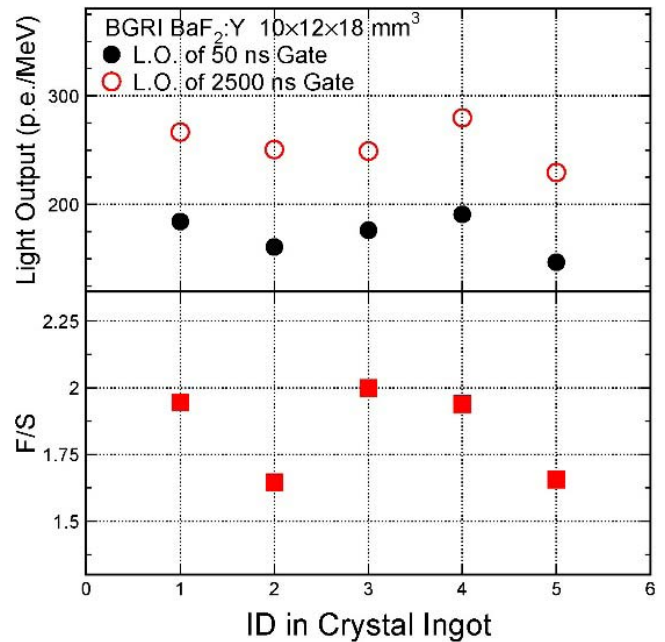
Fig. 14.   LO and F/S ratios for five samples cut adjacent to the long crystal. See Fig. 2 for their physical location within the ingot.

crystal [13], so that it be maybe ascribed to a disturbed Ce site. The transverse EWLT values in Fig. 12 also show that its optical quality varies along the crystal length, which may be improved by refining growth parameters.

Fig. 13 shows the transverse EWLT values as a function of the distance to the seed end for the $25 \times 25 \times 100$ mm^3 sample. Two dips were observed at 38 and 75 mm from the seed end for both the fast (top) and slow (bottom) components.

To further understand the dips observed in this long sample, five small samples of $10 \times 12 \times 18$ mm^3 cut adjacent to the

long crystal were measured. Fig. 14 shows their LO (top) and F/S ratios (bottom). We note that the F/S ratio decreases from the seed to the tail, and the samples 2 and 5, corresponding to 18–36 mm and 72–90 mm, respectively, in the long crystal, have a lower LO and F/S ratio. This is consistent with the low transverse EWLT values of the fast component observed in the long crystal. We conclude that these dips are caused by localized poor optical quality in the long ingot. Further improvements on the optical quality at the ultraviolet range may be achieved by refining growth parameters.

Fig. 15. LO as a function of the integration time for the long BaF$_2$:Y sample with the seed (top) and tail (bottom) end coupled to the PMT.

Fig. 16. LRU for the 100-mm long BaF$_2$:Y sample with the seed coupled to the PMT measured with 50 and 2500-ns (middle) integration time as well as their ratio (bottom).
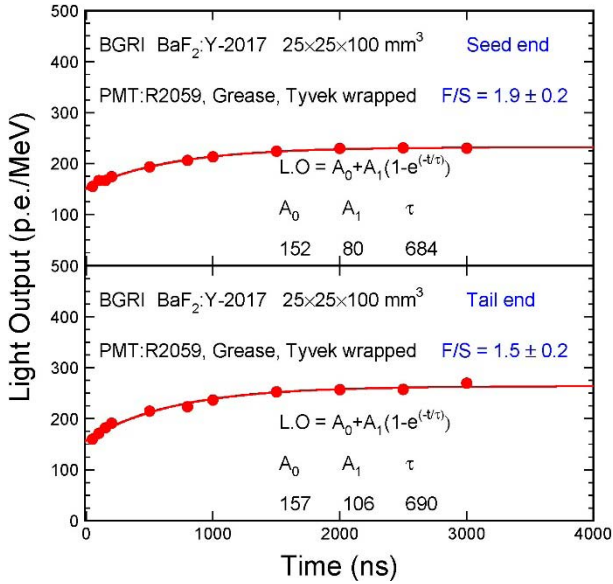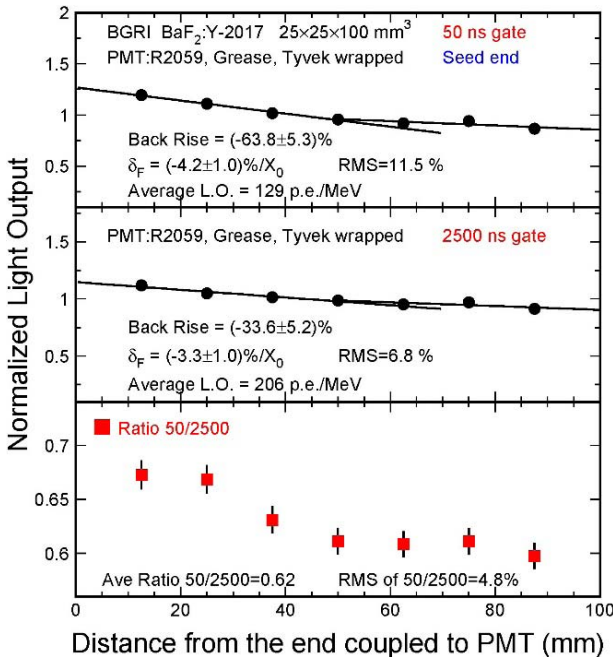
Fig. 15 shows the LO as a function of the integration time for the long BaF$_2$:Y sample with the seed (top) and tail (bottom) end coupled to the PMT. The F/S ratios are 1.9 and 1.5, respectively, at the seed and tail ends. Compared to undoped BaF$_2$ crystals, yttrium doping can effectively suppress the slow component and maintain the ultrafast component.

Fig. 16 shows the LRU measured with 50 (top) and 2500-ns integration time (middle) as well as their ratio (bottom) for the 100-mm-long BaF$_2$:Y sample. The root mean square (rms) of the LO values with 50-ns integration time is about 12%,

which is consistent with what observed in undoped BaF$_2$ crystals [30].

IV. CONCLUSION

We investigated a set of $\Phi 18 \times 21$ mm^3 BaF$_2$ cylinders grown at BGRI with yttrium doping level from 0 at.% to 7.0 at.%. Their scintillation performance, including XEL and transmittance spectra as well as LO and fast-to-slow ratios, demonstrates that yttrium doping reduces the slow scintillation component greatly while maintaining the intensity of the fast scintillation component unchanged. The best doping level is found to be about 5 at.%.

We further investigated scintillation performance for a $25 \times 25 \times 100$ mm^3 BaF$_2$:Y crystal and several small slices cut from a $\Phi 40 \times 160$ mm^3 ingot grown at BGRI with 5 at.% yttrium doping. An excellent correlation was observed between the LO of the fast component and the transmittance at 220 nm, indicating the importance of optical quality at the UV range for the ultrafast light. An F/S ratio of up to 4.5:1 and 2:1 is observed in small and large BaF$_2$:Y samples, respectively. This result is much better than the first 19-cm-long BaF$_2$:Y sample grown at SIC [15]. Further improvement is expected with improved optical quality by refining growth parameters.

BaF$_2$:Y crystals with suppressed slow component are important for applications in future HEP and nuclear physics experiments where ultrafast timing is required, such as the proposed the compact muon solenoid, MIP timing detector, at CERN [31], the Mu2e-II calorimeter [32] at Fermilab, and gigahertz (GHz) hard X-ray imaging for the proposed MaRIE project at LANL [33] as well as TOF-PET. Our investigations will continue to improve the optical quality of BaF$_2$:Y crystals and to understand their radiation hardness against γ-rays, protons, and neutrons.

REFERENCES

[1] Y. M. Aleksandrov, V. N. Makhov, P. A. Rodnyj, T. I. Syrejshchikova, and M. N. Yakimenko, "Intrinsic luminescence of BaF$_2$ at pulsed synchrotron radiation excitation," *Sov. Phys. Solid State*, vol. 26, no. 9, pp. 2865–2867, 1984.

[2] P. Dorenbos, R. Visser, J. Andriessen, C. W. E. van Eijk, J. Valbis, and N. M. Khaidukov, "Scintillation properties of possible cross-luminescence materials," *Nucl. Tracks Radiat. Meas.*, vol. 21, no. 1, pp. 101–103, 1993.

[3] V. N. Makhov, "Vacuum ultraviolet luminescence of wide band-gap solids studied using time-resolved spectroscopy with synchrotron radiation," *Phys. Scripta*, vol. 89, no. 4, Feb. 2014, Art. no. 044010.

[4] G. Pezzullo *et al.*, "Progress status for the Mu2e calorimeter system," *J. Phys., Conf. Ser.*, vol. 587, no. 1, 2015, Art. no. 012047.

[5] N. Atanov *et al.*, "Design and status of the Mu2e crystal calorimeter," *IEEE Trans. Nucl. Sci.*, vol. 65, no. 8, pp. 2073–2080, Aug. 2018.

[6] F. Yang, L. Zhang, and R.-Y. Zhu, "Gamma-ray induced radiation damage up to 340 Mrad in various scintillation crystals," *IEEE Trans. Nucl. Sci.*, vol. 63, no. 2, pp. 612–619, Apr. 2016.

[7] C. Hu *et al.*, "Proton-induced radiation damage in BaF$_2$, LYSO, and PWO crystal scintillators," *IEEE Trans. Nucl. Sci.*, vol. 65, no. 4, pp. 1018–1024, Apr. 2018.

[8] C. Hu *et al.*, "Neutron-induced radiation damage in BaF$_2$, LYSO/LFS and PWO crystals," presented at the Calor Conf., 2018.

[9] P. Schotanus, P. Dorenbos, C. W. E. van Eijk, and H. J. Lamfers, "Suppression of the slow scintillation light output of BaF$_2$ crystals by La^{3+} doping," *Nucl. Instrum. Methods Phys. Res. A, Accel. Spectrom. Detect. Assoc. Equip.*, vol. 281, pp. 162–166, Aug. 1989.

[10] C. L. Woody, P. W. Levy, and J. A. Kierstead, "Slow component suppression and radiation damage in doped BaF_2 crystals," *IEEE Trans. Nucl. Sci.*, vol. 36, no. 1, pp. 536–542, Feb. 1989.

[11] B. P. Sobolev, E. A. Krivandina, S. E. Derenzo, and W. W. Moses, "Suppression of BaF_2 slow component of X-ray luminescence in non-stoichiometric $Ba_{0.9}R_{0.1}F_{2.1}$ crystals (R=rare earth element)," *Proc. Mater. Res. Soc., Scintillator Phosphor Mater.*, vol. 348, pp. 227–283, 1994.

[12] N. Kawaguchi *et al.*, "Nd concentration dependence on the optical and scintillation properties of Nd doped BaF_2," *Opt. Mater.*, vol. 32, no. 10, pp. 1325–1328, Aug. 2010.

[13] F. Yang, J. Chen, L. Zhang, C. Hu, and R.-Y. Zhu, "La and La/Ce doped BaF_2 crystals for future HEP experiments at the energy and intensity frontiers part I," *IEEE Trans. Nucl. Sci.*, vol. 66, no. 1, pp. 506–511, Jan. 2019.

[14] F. Yang, J. Chen, L. Zhang, C. Hu, and R.-Y. Zhu, "La and La/Ce doped BaF_2 crystals for future HEP experiments at the energy and intensity frontiers part II," *IEEE Trans. Nucl. Sci.*, vol. 66, no. 1, pp. 512–518, Jan. 2019.

[15] J. Chen *et al.*, "Slow scintillation suppression in yttrium doped BaF_2 crystals," *IEEE Trans. Nucl. Sci.*, vol. 65, no. 8, pp. 2147–2151, Aug. 2018.

[16] J. H. Beaumont, W. Hayes, D. L. Kirk, and G. P. Summers, "An investigation of trapped holes and trapped excitons in alkaline earth fluorides," *Proc. Roy. Soc. London A, Math. Phys. Sci.*, vol. 315, pp. 69–97, Feb. 1970.

[17] E. Radzhabov, A. Istomin, A. Nepomnyashikh, A. Egranov, and V. Ivashechkin, "Exciton interaction with impurity in barium fluoride crystals," *Nucl. Instrum. Methods Phys. Res. A, Accel. Spectrom. Detect. Assoc. Equip.*, vol. 537, pp. 71–75, Jan. 2005.

[18] E. Radzhabov, M. Kirm, A. Egranov, A. Nepomnyachshikh, and A. Myasnikova, "Mechanism of exciton suppression in alkaline-earth fluorides doped with La, Y, Cd," in *Proc. SCINT*, 2005, pp. 60–63.

[19] A. S. Myasnikova, E. A. Radzhabov, and A. V. Egranov, "Extrinsic luminescence of $BaF_2:R^{3+}$ crystals ($R^{3+} = La^{3+}$, Y^{3+}, Yb^{3+})," *Phys. Solid State*, vol. 50, pp. 1644–1647, Sep. 2008.

[20] Z. Y. Wei, R. Y. Zhu, H, Newman, and Z. W. Yin, "Light yield and surface treatment of barium fluoride crystals," *Nucl. Instrum. Methods Phys. Res. B, Beam Interact. Mater. At.*, vol. 61, pp. 61–66, Jul. 1991.

[21] R.-Y. Zhu, "On quality requirements to the barium fluoride crystals," *Nucl. Instrum. Methods Phys. Res. A, Accel. Spectrom. Detect. Assoc. Equip.*, vol. 340, pp. 442–457, Mar. 1994.

[22] J. Chen, C. Hu, Y. Du, L. Zhang, and R.-Y. Zhu, "Optical and scintillation properties of BaF^2 crystals with 5at% Y-doping," presented at the IEEE NSS/MIC, 2018.

[23] R. T. Williams and K. S. Song, "The self-trapped exciton," *J. Phys. Chem. Solids*, vol. 51, no. 7, pp. 679–716, 1990.

[24] P. Dorenbos, R. Visser, R. Dool, J. Andriessen, and C. W. E. van Eijk, "Suppression of self-trapped exciton luminescence in La^{3+}- and Nd^{3+}-doped BaF_2," *J. Phys., Condens. Matter*, vol. 4, no. 23, pp. 69–97, 1992.

[25] R. Visser, P. Dorenbos, C. W. E. van Eijk, and H. W. D. Hartog, "Energy transfer processes observed in the scintillation decay of $BaF_2:La$," *J. Phys. Condens. Matter*, vol. 4, no. 45, pp. 8801–8812, 1992.

[26] R. Visser, P. Dorenbos, C. W. E. van Eijk, A. Meijerink, G. Blasse, and H. W. D. Hartog, "Energy transfer processes involving different luminescence centres in $BaF_2:Ce$," *J. Phys., Condens. Matter*, vol. 5, no. 11, pp. 1659–1680, 1993.

[27] C. Hu *et al.*, "Ultrafast inorganic scintillators for gigahertz hard X-ray imaging," *IEEE Trans. Nucl. Sci.*, vol. 65, no. 8, pp. 2097–2104, Aug. 2018.

[28] E. Loh, "Ultraviolet absorption spectra of Ce^{3+} in alkaline-earth fluorides," *Phys. Rev. J. Arch.*, vol. 154, no. 2, pp. 270–276, Feb. 1967.

[29] W. J. Manthey, "Crystal field and site symmetry of trivalent cerium ions in CaF_2: The C_{4v} and C_{3v} centers with interstitial-fluoride charge compensator," *Phys. Rev. B, Covering Condens. Matter Mater. Phys.*, vol. 8, no. 9, pp. 4086–4098, Nov. 1973.

[30] F. Yang, J. Chen, L. Zhang, and R. Zhu, "Development of BaF_2 crystals for future HEP experiments at the intensity frontiers," in *Proc. IEEE Nucl. Sci. Symp., Med. Imag. Conf. Room-Temp. Semiconductor Detect. Workshop*, Oct./Nov. 2016, pp. 1–4.

[31] T. Tabarelli de Fatis, "Precision timing studies and detector concept proposal," presentation given in the CMS general meeting, Nov. 2016.

[32] F. Abusalma *et al.*, "Expression of interest for evolution of the Mu2e experiment," 2018, *arXiv:1802.02599*. [Online]. Available: https://arxiv.org/abs/1802.02599

[33] C. W. Barnes *et al.*, "Technology risk mitigation research and development for the matter-radiation interactions in extremes (MaRIE) project," Los Alamos Nat. Lab., Los Alamos, NM, USA, Tech. Rep. LA-UR-17-26474, 2017.